On the galactic spiral arms nature as revealed by the kinematics of the stellar component

S. Roca-Fàbrega[1], **O. Valenzuela**[2], **F. Figueras**[1], **M. Romero-Gómez**[1], **H. Velázquez**[3], **T. Antoja**[4], **and B. Pichardo**[2]

[1] Departament d'Astronomia i Meteorologia and IEEC-UB, Institut de Ciències del Cosmos de la Universitat de Barcelona, Martí i Franquès, 1, E-08028 Barcelona, `sroca@am.ub.es`
[2] Instituto de Astronomía, Universidad Nacional Autonóma de Mexico, A.P. 70-264, 04510, México, D.F.
[3] Instituto de Astronomía, Universidad Nacional Autónoma de México, A. P. 877, 22800, Ensenada, México
[4] Kapteyn Astronomical Institute, University of Groningen, PO Box 800, 9700 AV, Groningen, The Netherlands

Abstract

N-body simulations conducted for kinematic analysis of stellar disk component -high number of disk particles, small time step and few parsecs spatial resolution - reveal two different behaviors for the spiral arm angular velocity. Whereas subdominant disk cases present transient spiral arm features corotating with particles, Milky Way like galaxies with higher disk/halo ratio develop a bar and transient spiral compatible with a pattern speed constant in radius. Both cases significantly depart from the TWA steady spiral arm density wave theory. Such results may have potential to be applied to arqueological studies of the Milky Way disks and high implication to the secular evolution of galaxies.

1 Introduction

Here we present preliminary results about the pattern speeds of the nonaxisymmetric structures in different N-body simulations, namely subdominant disk and Milky-Way like galxies. This is a topic of relevant importance nowadays.

An interesting debate about the corotating nature of spiral patterns has been recently opened (e.g. [5, 6]). Thus it is not clear how the arms and the bar are related. Pattern speed of these structures seem to show different values, none of them in corotation with the disk, leaving unclear spiral arms nature.

As mentioned above, we analyse the rotation of spiral patterns in different morphological type
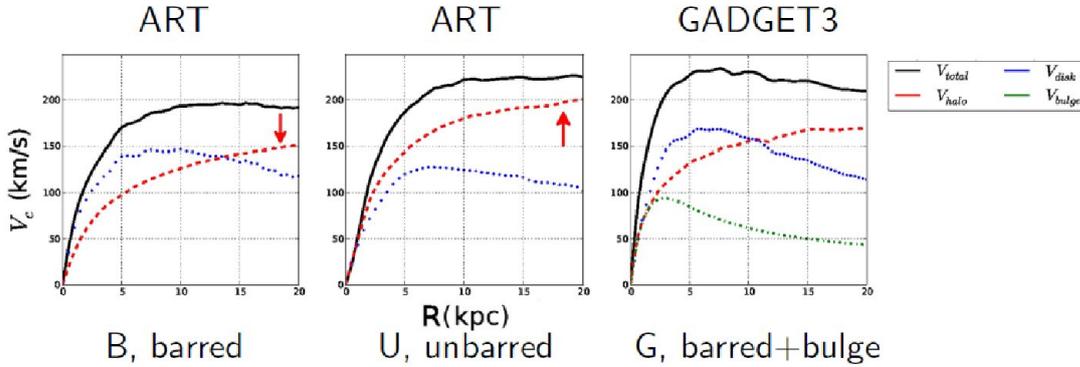
Figure 1: Initial circular velocity of models B (left), U (center) and G (right) , computed using the potential field. We show the total rotation curve (black solid) and disk (blue dotted), halo (red dashed) and bulge (green dot-dashed) contributions.

of galaxies, namely those with barred and unbarred disks, with and without bulge, looking for answers to some questions like: How do the results depend on the method used to derive the pattern speed? Do bars, indeed, drive spiral density waves?

2   N-body simulations

We have performed collisionless N-body simulations with ART [8] and GADGET3 [10] codes. The initial conditions have been generated using Hernquist method [7] for ART simulations and Widrow method for GADGET3 ones [13]. All the simulations we used are fully self-consistent , all of them have live disk and live dark matter halo.

We used the ART code to simulate barred and unbarred galactic models, labeled B and U, respectively. For these models we have used the multimass method to sample the halo particle distribution, which allows us to obtain the same results as using a higher number (N_{eff}) of particles [12]. In the case of barred models we have a stellar disk similar to the one observed for the MW with initial parameters as proposed by [3] (model K_{cb}). For U models we have a smaller disk than the ones for barred models and a massive and highly concentrated halo($M_d = 3.75 \cdot 10^{10} \, \text{M}_\odot$, $R_d = 4.0$ kpc, $M_h = 1.5 \cdot 10^{12} \, \text{M}_\odot$, $C = 18$), with these variations we get a disk that do not develops a bar. Furthermore we have used GADGET3 to simulate barred models -labeled G- with an additional bulge component with a Sersic profile ($R_b = 1.75$ kpc, $M_b = 8.57 \cdot 10^9 \, \text{M}_\odot$) and slightly different parameters from the barred case, for the disk and the halo ($M_d = 6.01 \cdot 10^{10} \, \text{M}_\odot$, $R_d = 3.0$ kpc, $M_h = 0.66 \cdot 10^{12} \, \text{M}_\odot$, $C = 10.4$). In Fig. 1 we show the rotation curve of these models. All the models presented here have from one to five million particles for the disk component and a spatial and temporal resolutions of about 11 pc and 50000 yrs.
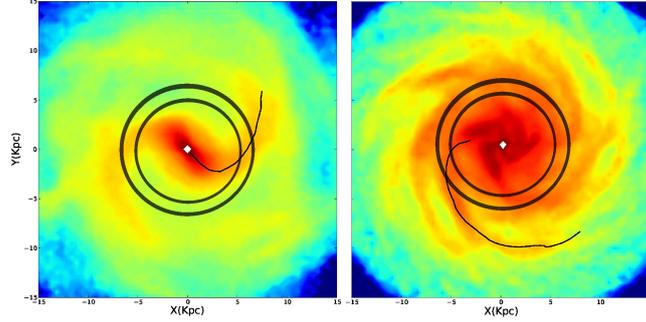
Figure 2: Density distribution of the models B1 (left) and U1 (right) after 900 Myr of evolution. The thin black solid line shows the locus of the spiral arms derived using Fourier analysis ($m = 2$ for B1 and $m = 4$ for U1). Spiral structure rotates clockwise in both models. The black solid circles show an example of cylinders where the Fourier modes position are computed.

3   Analysis tools

3.1   Tracing the density structures

We use two methods to trace the density peak of the spirals and the bar. The first method applies a spatial Fourier analysis over the azimuthal angle (see Eq. 2). The second method, labeled here the density peak method, is implemented following three steps. First, we generate a density map using SMOOTH[1] and we select the density cut where the spiral density peak is well traced. Second, we find the particles associated to the spiral structure using a Friends of Friends (FoF) clustering algorithm. The clustering parameters have been obtained iteratively. Finally, for the selected particles, we compute their mean position as a function of radius, thus providing the orientation of the structure. Both methods work in cylindrical shells equally spaced in galactocentric distance. Figure 2 shows an example of how well the spatial Fourier method traces the peak overdensities.

$$
\begin{aligned}
a_m(r) &= \sum_{i=1}^{N} \sin(m\phi_i) \\
b_m(r) &= \sum_{i=1}^{N} \cos(m\phi_i) \\
A_m(r) &= \sqrt{a_m^2 + b_m^2}
\end{aligned}
\tag{1}
$$

---

[1] N-body shop, University of Washington

3.2 Computing the pattern speed

We have implemented two substantially different methods for the computation of the angular speed of the spiral pattern. The first one, hereafter finite differences method (see Eq. 2), considers three consecutive snapshots for which the locus of the spiral has been derived and computes the rotation frequency by finite differences.

$$\omega_{(rad/Myr)} \quad = \quad \frac{\phi_{i+1} - \phi_{i-1}}{2 \cdot \Delta t} \tag{2}$$

$$\tilde{A}_m(\omega, r) \quad = \quad \sum_{T_1}^{T_2} e^{i\omega t}[b_m(r,t) + i \cdot a_m(r,t)]\Delta t \tag{3}$$

The second method uses spectrograms (see Eq. 3), proposed by [9]. In this case the temporal spectrum is obtained by taking the Fourier transform with respect to time. The sampling frequency, that is the time step between consecutive snapshots, has been selected to have a Nyquist frequency of $\sim 100 - 150$ km s^{-1} kpc^{-1}.

4   Results and discussion

In Fig. 3 we show the results of computing the angular speeds of $m = 2$ mode of barred models (left), and $m = 4$ of unbarred models (right). We show in top panels of this figure, the amplitude as a function of the temporal evolution of spatial Fourier modes 2, 3 and 4. We analyse the temporal range from 0.9 to 2.3 Gyr, which allows us to study several cycles of spiral creation and destruction. The spirals have a transient and recurrent nature and the amplitude in the unbarred case is significantly weaker than in the barred model. In the central panels we show the results obtained using the spectrograms method. We indicate the time interval used to make spectrograms as thick black dashed lines in the top panels. Finally in the bottom panels we show the angular speed computed using the finite differences method. We observe how the non-corotating behavior of spiral pattern in barred models is confirmed in different scenarios: first, when a different N-body code is used (GADGET3, in green, instead of ART, in red and blue) , second, when a bulge component (green) is added and third, when a model with five million particles in the disk is considered (blue). The results shown as red, blue and green lines, have been obtained applying the Fourier analysis plus finite differences to the few Myr covering the peak of maximum spiral amplitude (shown as dots in top panels). The blue dots show the results obtained using smooth method plus finite differences to a time instant of the five million particles simulation.

After making several analysis, using different techniques (i.e Fourier analysis, smooth routine, finite differences and spectrograms) and galactic models (different codes and initial conditions) we confirm that exists a truly distinct behavior between barred and unbarred models: whereas in barred models (left), the spiral pattern clearly rotates rigidly and faster than disk
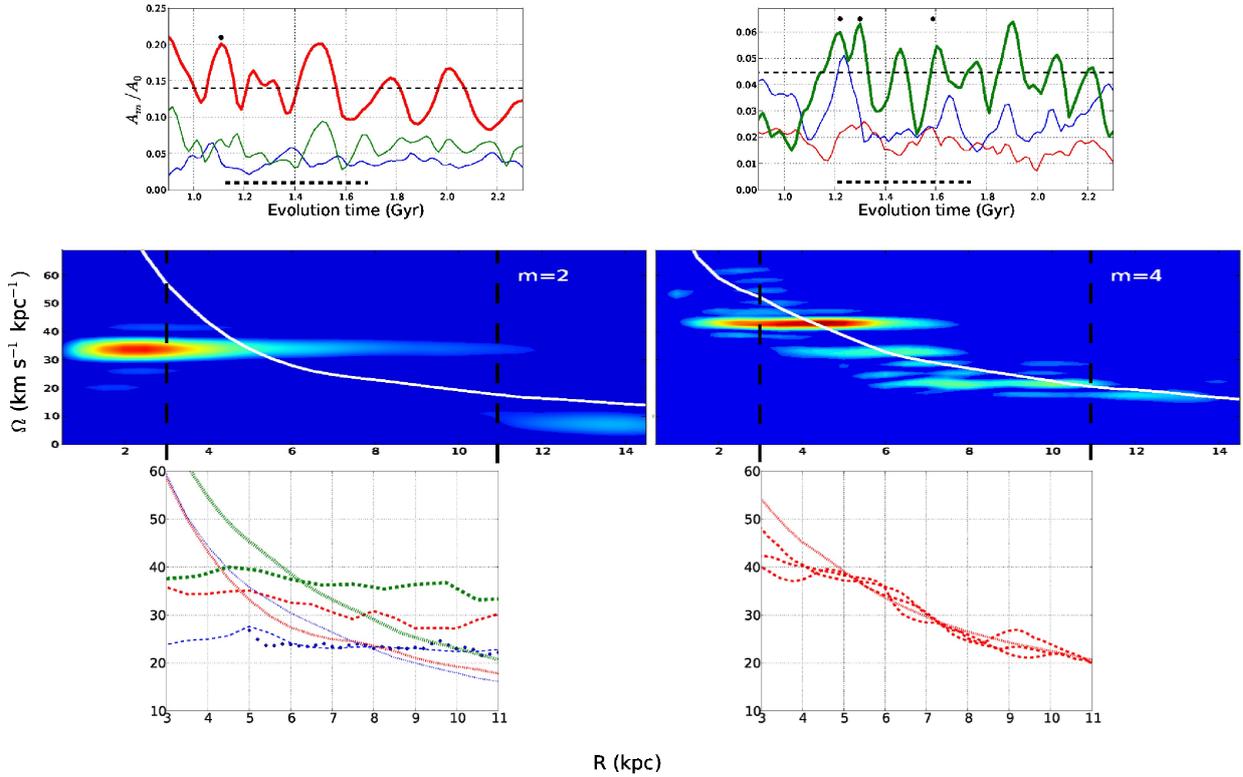
Figure 3: Results summary table for barred (left) and unbarred (right) models. Top: amplitudes as a functinon of time evolution for modes 2(red), 3(blue) and 4(green). Center: Results obtained using spectrograms method. Bottom: Results obtaining using Fourier+finite differences and smooth+finite differences method for single time instants.

particles ($R \geq 6$ kpc), unbarred models (right) show an almost corotating with disk 3-4 armed structure, behavior that is maintained through all galactocentric radii larger than ∼4.5 kpc.

Our results are robust to the selection of numerical parameters (time step, number of particles, time resolution) which highly reinforce our conclusions.
Note that although in our simulations the dominant spiral arms are most of the time connected to the bar, the actual situation in the MW may be more complex [1]. Work is in progress to analyse simulations including hydrodynamics in a realistic cosmological environment (HART, [4]). The main challenge for the next decade will be to compare them with the observational data. It is clear that the accurate astrometric data from the Gaia (ESA) mission will fill this gap. In order to be ready for this challenge, we shall adapt model independent tools to estimate pattern speeds like the one proposed by [11].

Acknowledgments

References

[1] Athanassoula, E. 2012, MNRAS, 426, 46

[2] Binney, J. & Tremaine, S. 2008, *Galactic Dynamics 2nd Edition.* Princeton

[3] Colín, P., Valenzuela, O., & Klypin, A. 2006, ApJ, 644, 687

[4] Colín, P., Avila-Reese, V., Vázquez-Semadeni, et al. 2011, ApJ, 713, 535

[5] Grand, R. J. J., Kawata, D., & Cropper, M. 2012a, MNRAS, 421, 1529

[6] Grand, R. J. J., Kawata, D., & Cropper, M. 2012b, MNRAS, 426, 167

[7] Hernquist, L. 1993, ApJ, 86, 389H

[8] Kravtsov, A. V., Klypin, A. A., & Khokhlov, A. M. 1997, ApJS, 111, 73

[9] Sellwood, J. A. & Athanassoula, L. 1986, MNRAS, 221, 195

[10] Springel V. 2008, MNRAS, 391, 1685

[11] Tremaine, S. & Weinberg, M. D. 1984, ApJ, 282, L5

[12] Valenzuela, O. & Klypin, A. A. 2003, MNRAS, 345, 406

[13] Widrow, L. M. & Dubinski, J. 2005, ApJ, 631, 838